

CODE NET: COVID-19 segmentation and detection via deep learning based networks

Fareesa Amina¹, Krishnanaik Vankdoth²

¹Department of Electronics and Communication Engineering, Bharatiya Engineering Science and Technology Innovation University (BESTIU), Gorantla Mandal, India

²Department of Electronics and Communication Engineering, Brilliant Grammar School Group of Institutions-Integrated Campus, Hyderabad, India

Article Info

Article history:

Received Jun 29, 2024

Revised Aug 11, 2025

Accepted Sep 1, 2025

Keywords:

Adaptive trilateral filter

Chest X-ray images

COVID-19 detection

Grad-CAM

Link Net

Reverse edge attention network

ABSTRACT

Humans with COVID-19 have an infectious condition that affects the respiratory system. In addition to more serious conditions, headaches may be fatal for those who have the disease. Our difficulty with COVID-19 detection stems from the unreliability of computed tomography (CT) and magnetic resonance imaging (MRI) scans in identifying lung abnormalities. COVID-19 detection is a time-consuming process. In this research, a novel CODE NET model is proposed for the detection of COVID-19 virus from the gathered lung chest X-ray (CXR) images. The images are pre-processed utilizing an adaptive trilateral filter to improve the quality of the images. A reverse edge attention network (RE-Net) uses enhanced images to segment the CXR images for accurate virus detection. The segmented images are fed into a Link Net to extract relevant features and classify the COVID-19 cases. The classified cases are fed into the Grad-CAM model to generate heat maps for accurately detecting the virus. According to the result, the proposed model attains 99.75% of accuracy rate for the COVID-19 detection. The proposed CODE NET enhances the overall accuracy by 1.78%, 1.51%, and 2.20% over combined domain features-random forest (CDF-RF), Bayes-SqueezeNet, and bidirectional long short-term memory (Bi-LSTM) respectively.

This is an open access article under the [CC BY-SA](https://creativecommons.org/licenses/by-sa/4.0/) license.



Corresponding Author:

Fareesa Amina

Department of Electronics and Communication Engineering,

Bharatiya Engineering Science and Technology Innovation University (BESTIU)

Gownivaripalli, Gorantla Mandal, Sri Satya Sai District, Andhra Pradesh, India

Email: fareesaameena@gmail.com

1. INTRODUCTION

The global coronavirus infection that caused the pandemic was officially named COVID-19 in March 2020. When an infected individual coughs or sneezes, release respiratory droplets that are then dispersed by the coronavirus [1]. These droplets have the potential to contaminate surfaces even more, spreading the infection. Individuals with chronological problems and the elderly are particularly vulnerable to coronavirus infection. In an effort to stop the cycle and stop the pandemic from spreading, numerous nations have locked their citizens and closed their borders [2], [3]. The century-long pandemic sickness known as COVID-19, or corona virus, has spread quickly throughout the world's population in the twenty-first century. According to recent data, COVID-19 afflicted over 72 million people globally and claimed the lives of about 1.5 million of them. Wuhan, a city in Eastern China, had an increase in COVID-19 widespread in December 2019, which turned into a major calamity in the early months of 2020 [4], [5]. This virus typically causes fever, dry coughs, and breathing difficulties when it affects the respiratory system. The computed tomography (CT) and chest

X-ray (CXR) are essential for predicting COVID-19 infection. Aside from the time needed for CT cleaning and the 12-hour real time-polymerase chain reaction (RT-PCR) test, a patient's CXR takes 15 minutes, and the equipment is frequently unavailable [6], [7]. However, CT scans [8] are widely accessible and take only 15 seconds for a patient. Nowadays deep learning (DL) [9] models are playing an important role in demonstrating outstanding performance for medical image analysis [10].

Researchers most frequently utilize artificial intelligence and DL techniques to identify coronavirus infection in CT images [11]. DL has shown significant promise for detecting COVID-19 [12]. However, several limitations and challenges hinder its effectiveness and widespread adoption in clinical settings [13], [14]. Patients and healthcare providers might mistrust a system that delivers results too quickly, perceiving it as less reliable or less rigorous [15], [16]. Recent studies have explored the use of DL methods for COVID-19 identification, summarizing various approaches. Okashi *et al.* [17] developed a method combining spatial and transform domain features from CT scans, achieving nearly 98% accuracy using CDF-RF based features. Ahmed *et al.* [18] suggested an IoT-based DL algorithm using faster regional convolutional neural network (Faster-RCNN) with ResNet-101, reaching 98% detection accuracy. Ucar and Korkmaz [19] suggested a COVIDiagnosis-Net based on Deep Bayes-SqueezeNet to automatically identify COVID-19 cases from X-ray images. This suggested model attains the overall accuracy of 98.26% for COVID-19 classification. Karthik *et al.* [20] suggested a CNN approach for COVID-19 recognition from CXR images, attaining a reliability rate of 99.80%. Yang *et al.* [21] suggested a generative adversarial network (GAN) and weakly-supervised method for lesion localization, while Akyol and Şen [22] recommended a bidirectional long short-term memory (Bi-LSTM) framework for COVID-19 and no-finding case identification, achieving 97.6% accuracy. Gülmez [23] utilized a genetic algorithm to optimize an Xception-based neural network, yielding accuracies of 0.996, 0.989, and 0.924 on different datasets. Finally, Abubakar *et al.* [24] combined DL and histogram of oriented gradient (HOG) features with SVM classifiers, with VGG-16+HOG attaining a 99.4% reliability rate. Several challenges have been identified in existing DL models for COVID-19 detection including limited generalizability due to reliance on specific often small or imbalanced datasets which can distort performance metrics. While many models report high accuracy but they frequently struggle to distinguish COVID-19 from CXR images. To overcome these issues, a novel DL based CODE NET model is proposed for the efficient detection of COVID-19 using CXR images. The following is the proposed model's primary contribution.

- A novel DL based CODE NET is proposed for the detection of COVID-19 virus from the gathered lung CXR images.
- The input images are pre-processed utilizing an adaptive trilateral filter to improve the quality of the images.
- A RE-Net uses enhanced images to segment the CXR images for accurate virus detection.
- The segmented images are fed into a Link Net to extract relevant features and classify the COVID-19 kinds.
- The classified images are put into the Grad-CAM model to generate heat maps for accurately detecting the virus.

This paper was prepared in the following manner. The proposed CODE NET is offered in section 2, the findings of the study are exposed in section 3, the conversation is outlined in section 4, and the conclusion is offered in section 5.

2. PROPOSED METHOD

In this research, a novel DL based CODE NET is proposed for the detection of COVID-19 virus. The input images are pre-processed utilizing adaptive trilateral filter. A reverse edge attention network (RE-Net) uses enhanced images to segment the CXR images for accurate virus detection. The segmented images are fed into an Link Net to extract relevant features and classify the COVID-19 cases. Figure 1 displays the schematic illustration of the suggested CODE NET.

2.1. Data pre-processing

The input medical images are pre-processed utilizing the AT filter to remove noise artifacts. It implements the guiding principles of the bilateral filter. The issue of high-gradient zones being ineffectively filtered by bilateral filters be resolved by using a trilateral filter under tilting. When a bilateral filter is applied to the image data, p should average highly related surrounding pixels and eliminate dissimilar pixels, yielding the tilting angle h_θ of a trilateral filter given h_θ at the target pixel.

$$h_\theta(q) = \frac{1}{l_\theta} \sum_q \sum_p f_p e(q, p) z(f_q, f_p) \quad (1)$$

When the kernel is tilted, the trilateral filter's $e(\cdot)$ and $z(\cdot)$ functions become non-orthogonal. In (2) establishes the value of each pixel at this plane.

$$j(q, p) = f(q) + h_{\theta} \cdot (||q - p||) \quad (2)$$

Where $||q - p||$ is the multidimensional spacing between q and $f(q)$, is represented by q at a target pixel, and h_{θ} is the tilting angle. To find the output of a trilateral filter, the resulting image is first passed through a bilateral filter, and then the value j is removed from the surrounding area of the target pixel.

$$f_o(q) = f_{in}(y) + t(y)\Delta \quad (3)$$

Where Δ is the spatial distance between pixels q and p , and $f_o(q)$ is the output function. Tilting improves the filter's capacity to smooth high gradient zones. It is insufficient because trilateral filter failure will only occur when tilting occurs in areas with notable gradient variations.

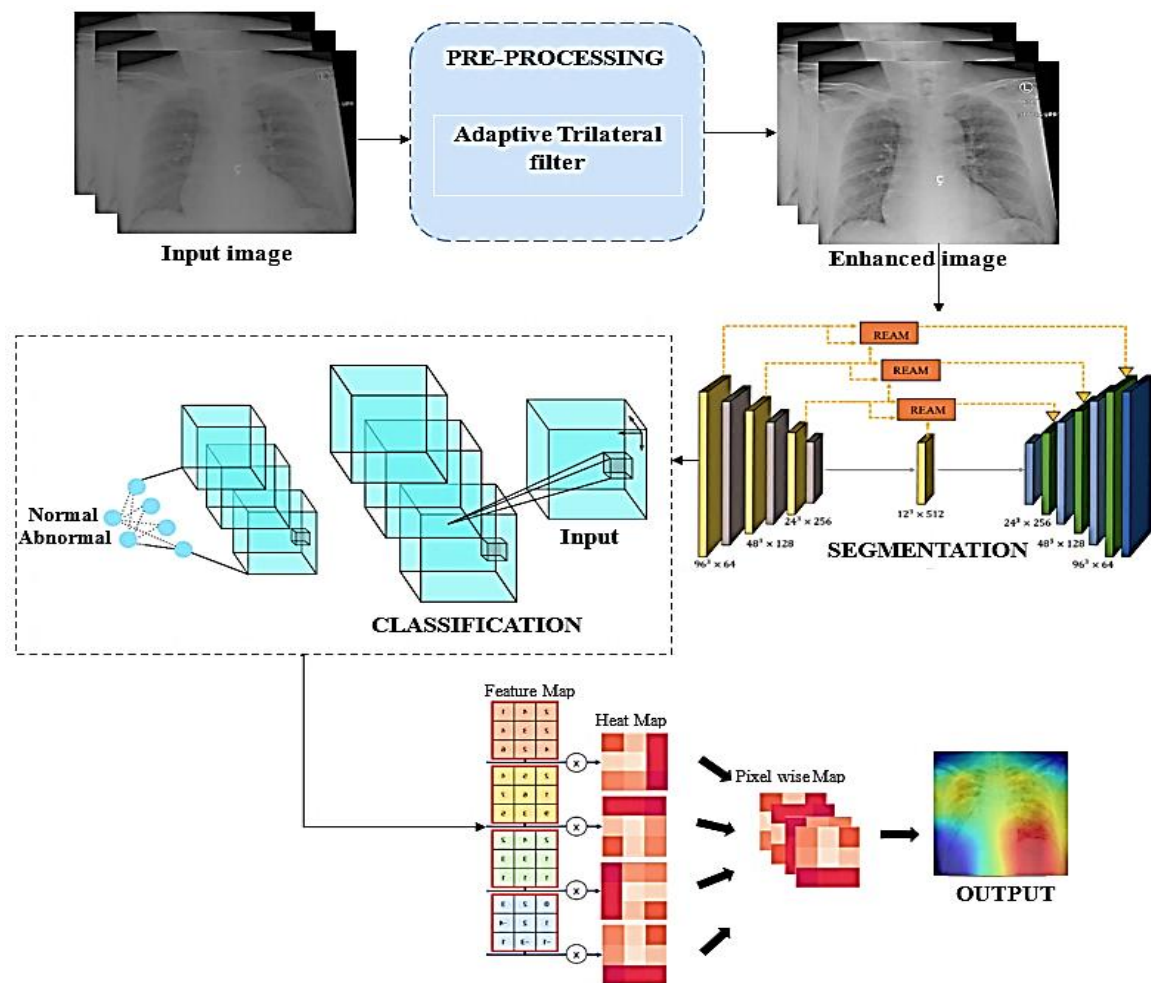


Figure 1. Schematic illustration of the proposed CODE NET

2.2. Segmentation

This section describes the RE-Net [25] to segment the CXR images for accurate virus detection. The encoder module and the decoder module are the binary phases of the proposed Reverse-Net. Each of the four encoding phases in the encoder module is based on a ResNet Block. The feature maps from the encoder module are passed to the decoder module to aid in decoding. The next step is to retrieve edge information from encoder layers by inserting a REAN in a skip relationship.

The features produced in the $(j - 1)^{th}$ encoder step is indicated by the notation $c_j \in K^{o*f*d}$. Initially, the features are fused into a single channel using a $1 \times 1 \times 1$ convolution. The features are then up sampled to provide $c_j \in K^{o*f*d}$, which is the results of $(j - 1)^{th}$ encoder phase. To obtain the accurate weight $f_j - 1$ in the $(j - 1)^{th}$ encoder step, just eliminate the up sampled forecast from j^{th} stage.

$$f_j - 1 = 1 - s(c_j) = 1 - \frac{1}{1+c^{-k}} \quad (4)$$

The notation $a_j \in K^{i*j*l*o}$ indicates the features created in the $(j-1)^{th}$ encoder phase. Therefore, edge feature $(j-1)^{th}$ is expressed and recorded as follows using element-wise multiplication:

$$C_j - 1 = a_j - 1 * f_j - 1 \quad (5)$$

Once the edge features are summed with $a_j - 1$, are added to the decoder's features at the proper point via skip connection. Alternatively, REAN suggests that additional edge information becomes available in the feature map following concatenation at the same place, hence enhancing the detection step.

2.3. Link Net

The encoder and decoder blocks make up Link Net framework to deconstruct and rebuild the image, respectively. The images then go through a couple convolutional layers. The model's classification of cerebral palsy is its intended use. In real time, Link Net functions as a semantic segmentation network. This preserves a significant portion of the image's spatial information. The method involves directly connecting the shallow feature map of the encoder module to the decoder module of the same size. This method speeds up computation without sacrificing precision by reducing the need for unnecessary computations and parameters by using the exact position data from the shallow layer. The architecture of the suggested Link Net demonstrates in Figure 2.

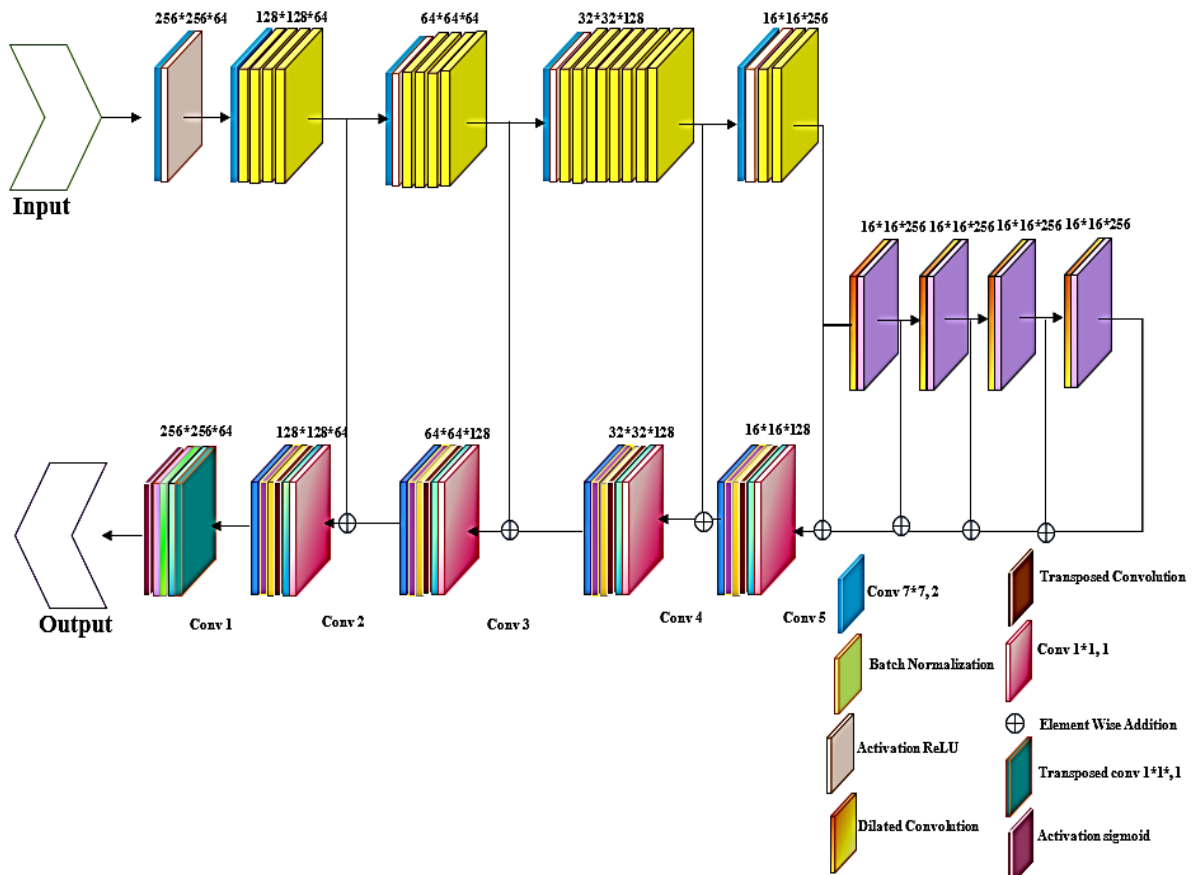


Figure 2. Architecture of the proposed Link Net

In dilated convolutions, the dilated rate dil_i indicates that the feature map has been subsampled by a factor of $dil_i - 1$ or that $dil_i - 1$ zeros have been inserted between the kernel weights. The 1×1 dilated kernel of size $sz_i \times sz_i$, resulting dil_i -dilated convolution kernel is given by (6).

$$\widehat{sz}_i = sz_i + (sz_i - 1) \times (dil_i - 1) = dil_i \times (sz_i - 1) + 1 \quad (6)$$

Let y be the convolution in the t^{th} layer ($t=1, 2, \dots, F$). The filter dimension of each dilated layer at dil_i is represented by n_p , which is given in (7).

$$\begin{cases} n_{pt} = y_{t-1} \times n_{pt} + s_{i_{t-1}} \widehat{y}_{t-1} \\ n_p = 1 \end{cases} \quad (7)$$

In terms of pixel-wise operation, the Link Net design is very different from neural networks. The relationship between the encoder and decoder is what makes it special. It is difficult to retrieve spatial information from the encoder's output once it has been lost during decoding. Non-trainable pooling indices serve as the link between the encoder and decoder in Link Net. This connection restores spatial data that was lost during encoding and is essential for the up-sampling process of the decoder. Compared to previous architectures, this approach helps create a more effective network for real-time cerebral palsy categorization.

2.4. Visualization using Grad-CAM

Grad-CAM is a guided propagation method for accessible classes that visualizes key regions. By sending the gradient of any chosen class into the final CNN layer, it highlights regions of the image for detection. Grad-CAM is computed by first determining the gradient of the class c score, or $\frac{\partial r^g}{\partial m^h}$, in relation to a convolutional layer feature map activation y^h . By pooling these gradients globally over the width and height dimensions, the neuron significance weights (t) are derived ((8) and (9)).

$$t_h^g = \frac{1}{b} \sum r \sum sz \frac{\partial r^g}{\partial m^h} \quad (8)$$

Furthermore, a combination of feature maps is used to compute the Grad-CAM heatmap, which is subsequently followed by *relu*.

$$y_{\text{Grad-CAM}} = \text{relu} \sum_h f_h^g y^h \quad (9)$$

Grad-CAM uses the gradient of the parameter of the final neural layer to calculate the degree of influence (shown by a heatmap) for each part of the images. The Grad-CAM technique is applied by first creating the sigmoid heatmap and then adding the input image. where t stands for the importance of the neuron and g for the class score.

3. RESULT AND DISCUSSION

In this section, the effectiveness of the suggested model is estimated utilizing MATLAB-2019b. The raw CXR images are extracted using the COVIDx dataset. For evaluating the performance, the recall, specificity, precision, F1-score, accuracy, and accuracy are utilized to generate the test sample analysis.

Figure 3 displays the COVIDx dataset visualization produced by the proposed approach. The input CXR image (column 1) is pre-processed. The enhanced images are segmented using RE-Net (column 3). The CXR images are supplied into the extraction process simultaneously (column 4) for categorizing the cases of COVID-19 (column 5). Finally based on the classification result the images are visualized (column 6) to enhance the reliability rate.

3.1. Performance analysis

The assessment metrics including F1-score, precision, recall, and accuracy were employed to assess the performance of the suggested approach for identifying the COVID-19.

$$\text{Accuracy} = \frac{T_r \text{Pos} + T_r \text{Neg}}{T_r \text{Pos} + T_r \text{Neg} + F_{al} \text{Pos} + F_{al} \text{Neg}} \quad (10)$$

$$\text{Precision} = \frac{T_r \text{Pos}}{T_r \text{Pos} + F_{al} \text{Pos}} \quad (11)$$

$$\text{Recall} = \frac{T_r \text{Pos}}{T_r \text{Pos} + F_{al} \text{Pos}} \quad (12)$$

$$F1\ Score = \frac{2PR}{P_r + R_e}$$

True positives and negatives of images are indicated by $T_r P_{os+}$ and $T_r N_{eg-}$, while false positives and negatives are shown by $F_{al} P_{os+}$ and $F_{al} N_{eg-}$. When assessing the precision of medical image segmentation algorithms to segment macular edema, the DI is a frequently employed statistic. It provides high-quality images with improved segmentation accuracy by measuring the overlap between the segmented regions in the image. The JI is a statistical technique used to assess the consistency and range of data sources.

$$DI = \frac{2T_p}{F_p + 2T_p + F_{ngt}} \quad (13)$$

$$JI = \frac{T_p}{T_p + F_{ngt} + F_p} \quad (14)$$

True negatives and positives of images are signified by T_p and T_{ngt} , while false positives and negatives are showed by F_p and F_{ngt} .

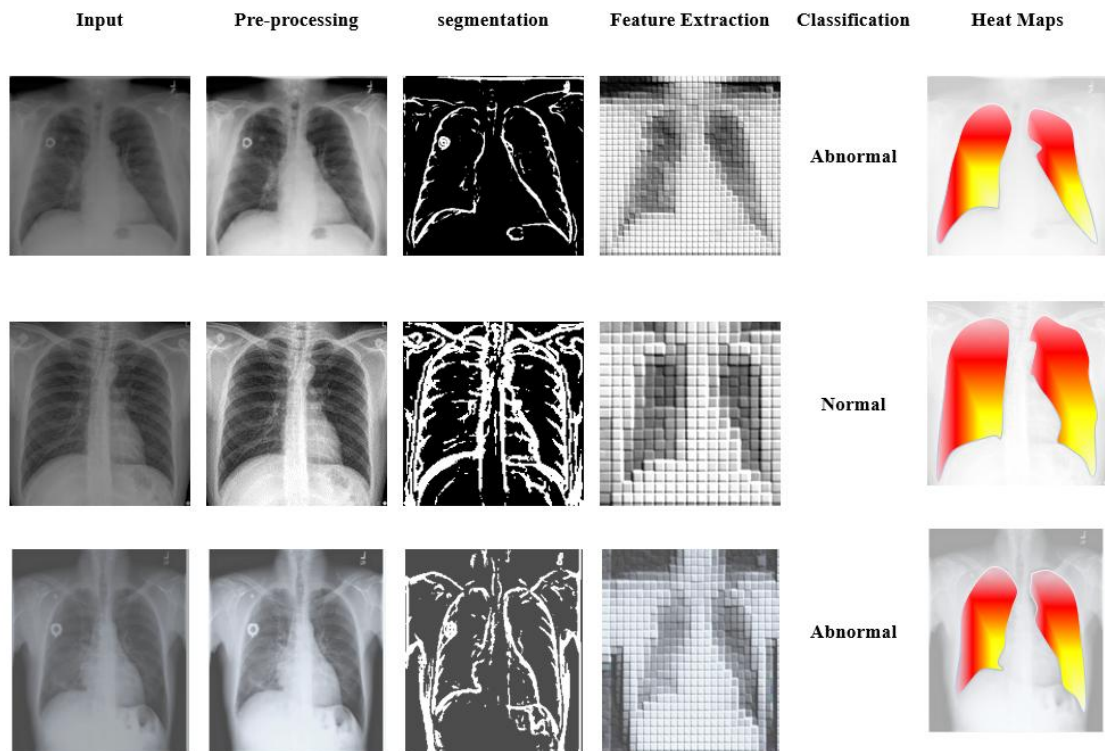


Figure 3. Experimental result of the proposed CODE-NET

Table 1 illustrates how well the suggested model finds COVID-19. The suggested model achieves 99.75% accuracy using the COVIDx dataset. Furthermore, it obtains scores of 96.19%, 96.03%, and 96.82% for recall, F1-score, and total precision, respectively.

Table 1. Performance evaluation of the CODE-NET model

Classes	F1-score	Precision	Accuracy	Recall
Normal	96.87	96.21	99.78	96.56
Abnormal	95.19	97.43	99.73	97.82

The accuracy graph in Figure 4 is estimated using the accuracy range and 100 epochs. As the number of epochs rises, the accuracy also rises. Figure 5 displays the loss range, showing that the loss decreases with increasing epochs. The proposed model achieves an outstanding level of COVID-19 recognition accuracy using CXR image. The results showed that the suggested has a low error rate and a 99.85% classification accuracy based on 100 training epochs.

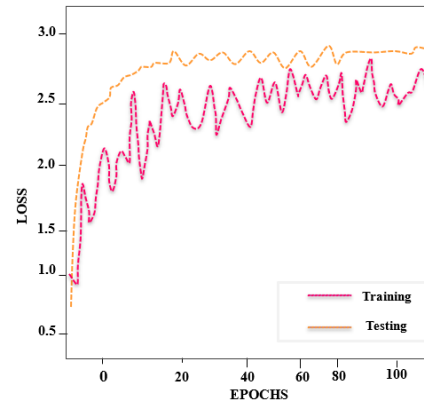
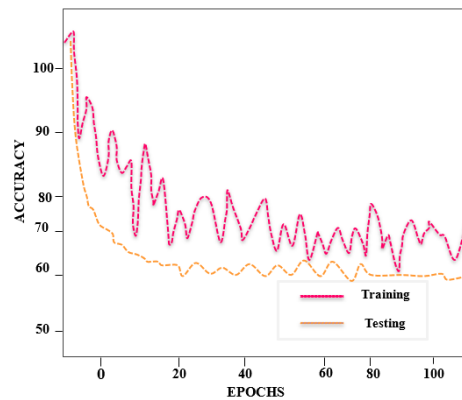


Figure 4. Accuracy graph of the CODE-NET model Figure 5. Loss graph of the proposed model

3.2. Comparative analysis

The suggested approach was associated with DL models on the basis of COVID-19 detection performance criteria in this comparison evaluation. The efficiency of existing procedures was examined to demonstrate that the CODE-NET model is more efficient in the development of COVID-19 detection. Table 2 shows a contrast of alternative segmentation models for COVID-19 recognition.

Table 2 compares the efficiency parameters of various segmentation techniques with the state-of-the-art networks. In assessment to N-Net, U-Net, and SegNet, the RE-Net enhances the Jaccard index by 3.12%, 17.03%, and 25.57%, respectively. Compared to N-Net, U-Net, and SegNet, the RE-Net rises the Dice index by 12.89%, 6.01%, and 7.27%. However, the RE-Net outperformed conventional segmentation networks in terms of performance.

Table 2. Comparison of segmentation approaches

Methods	Accuracy	Recall	Precision	F1-score	Jaccard index	Dice index
N-Net	93.86	92.24	88.97	93.27	93.67	80.67
U-net	93.15	86.25	88.22	87.39	79.76	87.55
SegNet	94.35	92.67	93.25	92.15	71.22	86.29
RE-Net (ours)	99.75	97.19	96.82	96.03	96.79	93.56

According to Table 3, the proposed Link Net is higher than that of the classic networks like MobileNet, GoogleNet, and RegNet. Link Net maintains 99.42% high accuracy ranges. Reg Net achieves an accuracy rate that is more efficient than that of existing approaches. The proposed Link Net improves its accuracy by 3.16%, 4.52%, and 2.41% better than MobileNet, GoogleNet, and RegNet respectively.

Table 3. Comparison of various networks

Techniques	Precision	F1-score	Recall	Accuracy
Mobile Net	90.31	95.87	94.29	96.59
Google Net	93.51	94.43	94.67	95.23
Reg Net	95.19	96.79	95.78	97.34
Proposed Link Net	96.03	96.82	97.19	99.75

According to Table 4, the CODE-NET approach enhances the accuracy of 1.78%, 1.51%, and 2.20% over CDF-RF, Bayes-SqueezeNet, and Bi-LSTM models. Nevertheless, the preceding networks did not yield better fallouts than the suggested model. As a result, the predicted results of the proposed CODE-NET attain the highest accuracy of 99.75% by surpassing all other approaches for COVID-19 recognition.

Table 4. Comparison of the proposed model with the existing models

Authors	Techniques	Accuracy (%)
Okashi <i>et al</i> [17]	CDF-RF	98.0
Ucar and Korkmaz [19]	Bayes-SqueezeNet	98.26
Akyol and Sen [22]	Bi-LSTM	97.6
Proposed method	CODE-NET	99.75

3.3. Discussion

In this work, the goal is to achieve accurate and efficient detection of COVID-19 cases from CXR images. For the experimental analysis, we used the COVIDx dataset for the detection of COVID-19. The results were assessed utilizing multiple assessment parameters with accuracy, precision, recall, and F1-score. Table 1 presents the evaluation metrics for the CODE-NET model across normal and abnormal classes. The suggested model achieves 99.75% accuracy using the COVIDx dataset. Furthermore, it obtains scores of 96.19%, 96.03%, and 96.82% for recall, F1-score, and precision, respectively. The training and testing graphs are demonstrated in Figures 4 and 5, the proposed model achieves an outstanding level of COVID-19 recognition accuracy using CXR image. The results showed that the suggested has a low error rate and a 99.85% classification accuracy based on 100 training epochs. Table 3 compares various networks based on F1-score, accuracy, recall, specificity, and precision. The proposed Link Net outperforms MobileNet, GoogleNet, and RegNet achieving the highest metrics across all categories, with an accuracy of 99.75% and a F1-score of 96.82%. Table 4 compares the accuracy of existing approaches with the CODE-NET framework. CODE-NET achieves the highest accuracy at 99.75%, outperforming other methods such as CDF-RF (98.0%), Bayes-SqueezeNet (98.26%), and Bi-LSTM (97.6%). From this analysis, the CODE-NET attains high accuracy with low complexity for detecting COVID-19 in the early stages.

4. CONCLUSION

In this research, a novel DL based CODE-NET approach is proposed for the recognition of COVID-19 virus. The pre-processing step with an adaptive trilateral filter ensures improved image quality, which is crucial for subsequent analysis. The RE-Net effectively segments the CXR images enhancing the precision of virus detection. Feature extraction and classification are robustly handled by the Link Net, ensuring accurate case categorization. Finally, the Grad-CAM model provides valuable heat maps that facilitate precise localization of the virus, thereby enhancing diagnostic accuracy. The performance of the proposed model was evaluated utilizing accuracy, F1-score, precision, recall, dice index, and Jaccard index. The proposed CODE-NET model achieved a notable accuracy rate of 99.75% and a dice index of 93.56% for detecting COVID-19. The RE-Net improved segmentation performance significantly with enhancements in the JI by 3.12%, 17.03%, and 25.57% over N-Net, U-Net, and SegNet, and in the DI by 12.89%, 6.01%, and 7.27% compared to the same models. Additionally, the Link Net demonstrated superior feature extraction surpassing MobileNet, GoogleNet, and RegNet by 3.16%, 4.52%, and 2.41%, respectively. The CODE-NET approach improved accuracy by 1.78%, 1.51%, and 2.20% over CDF-RF, Bayes-SqueezeNet, and Bi-LSTM models. The limitation of the proposed method is its potential difficulty in handling diverse image qualities and variations across different CXR sources. The complexity of the model may also result in higher computational demands and extended processing times. Future work could involve improving the model's robustness to image quality variations, optimizing computational efficiency, and integrating the system for real-time clinical use.

ACKNOWLEDGMENTS

The author would like to express their heartfelt gratitude to the supervisor for his guidance and unwavering support during this research for their guidance and support.

FUNDING INFORMATION

No financial support.

AUTHOR CONTRIBUTIONS STATEMENT

This journal uses the Contributor Roles Taxonomy (CRediT) to recognize individual author contributions, reduce authorship disputes, and facilitate collaboration.

Name of Author	C	M	So	Va	Fo	I	R	D	O	E	Vi	Su	P	Fu
Fareesa Amina	✓	✓	✓	✓	✓	✓		✓	✓	✓			✓	
Krishnanaik Vankdoth	✓		✓	✓			✓			✓	✓	✓	✓	✓

C : Conceptualization

M : Methodology

So : Software

Va : Validation

Fo : Formal analysis

I : Investigation

R : Resources

D : Data Curation

O : Writing - Original Draft

E : Writing - Review & Editing

Vi : Visualization

Su : Supervision

P : Project administration

Fu : Funding acquisition

CONFLICT OF INTEREST STATEMENT

The authors declare that they have no known competing financial interests or personal relationships that could have appeared to influence the work reported in this paper.

INFORMED CONSENT

We certify that we have explained the nature and purpose of this study to the above-named individual, and we have discussed the potential benefits of this study participation. The questions the individual had about this study have been answered, and we will always be available to address future questions.

ETHICAL APPROVAL

Our research guide reviewed and ethically approved this manuscript for publishing in this Journal.

DATA AVAILABILITY

Data sharing not applicable to this article as no datasets we regenerated or analyzed during the current study.




REFERENCES

- [1] S. Assaad *et al.*, "High mortality rate in cancer patients with symptoms of COVID-19 with or without detectable SARS-COV-2 on RT-PCR," *European Journal of Cancer*, vol. 135, pp. 251-259, 2020, doi: 10.1016/j.ejca.2020.05.028.
- [2] A. Santos *et al.*, "COVID-19 impedimetric biosensor based on polypyrrene nanotubes, nickel hydroxide and VHH antibody fragment: specific, sensitive, and rapid viral detection in saliva samples," *Materials Today Chemistry*, vol. 30, pp. 101597, 2023, doi: 10.1016/j.mtchem.2023.101597.
- [3] D. Radha, "Analysis of COVID-19 and pneumonia detection in chest X-ray images using Deep Learning," in *2021 International Conference on Communication, Control and Information Sciences (ICCISc)*, 2021, doi: 10.1109/iccisc52257.2021.9484888.
- [4] M. J. Horry *et al.*, "Covid-19 detection through transfer learning using Multimodal Imaging Data," *IEEE Access*, vol. 8, pp. 149808–149824, 2020, doi: 10.1109/access.2020.3016780.
- [5] Z. Hamidi, S. Jabraeili-Siahrour, Y. Taati-Alamdari, P. S. Aghbash, A. Shamekh, and H. B. Baghi, "A comprehensive review of COVID-19 symptoms and treatments in the setting of autoimmune diseases," *Virology Journal*, vol. 20, no. 1, pp.1, 2023, doi: 10.1186/s12985-023-01967-7.
- [6] Z. Khoshkam *et al.*, "Recovery scenario and immunity in COVID-19 disease: A new strategy to predict the potential of reinfection," *Journal of Advanced Research*, vol. 31, pp. 49-60, 2021, doi: 10.1016/j.jare.2020.12.013.
- [7] M. Giovanetti *et al.*, "Epidemic history and evolution of an emerging threat of international concern, the severe acute respiratory syndrome coronavirus 2," *Journal of Medical Virology*, vol. 95, no. 8, p. e29012, 2023, doi: 10.1002/jmv.29012.
- [8] L. Chang, M. Mohsin, and W. Iqbal, "Assessing the nexus between COVID-19 pandemic-driven economic crisis and economic policy: lesson learned and challenges," *Environmental Science and Pollution Research*, vol. 30, no. 9, pp. 22145-22158, 2023, doi: 10.1007/s11356-022-23650-0.
- [9] W. R. Ibrahim and M. R. Mahmood, "COVID-19 detection based on convolution neural networks from CT-scan images: a review," *Indonesian Journal of Electrical Engineering and Computer Science*, vol. 29, no. 3, pp. 1668-1677, 2023, doi: 10.11591/ijeecs.v29.i3.pp1668-1677.
- [10] V. Hemamalini, L. Anand, S. Nachiyappan, S. Geeitha, and V. R. Motupalli, "Integrating Bio Medical sensors in Detecting hidden Signatures of COVID-19 with Artificial Intelligence," *Measurement*, 2022, doi: 10.1016/j.measurement.2022.111054.
- [11] D. S. Dakshina, D. R. Valiaveetil, and A. Bindhu, "Alzheimer disease detection via deep learning-based shuffle network," *International Journal of Current Bio-Medical Engineering*, vol. 01, no. 01, pp. 09-15, 2023, doi: 10.5121/ijcnc.2023.15601.
- [12] A. Agasthian, R. Pamula, and L. A. Kumaraswamidhas, "Integration of monitoring and security based deep learning network for wind turbine system," *International Journal of System Design and Computing*, vol. 01, no. 01, pp. 11-17, 2023, doi: 10.1007/s12083-022-01394-5.
- [13] A. Shoeibi *et al.*, "Automated detection and forecasting of covid-19 using deep learning techniques: A review," *Neurocomputing*, 2024, doi: 10.1016/j.neucom.2024.127317.
- [14] Nurjahan, M. Mahbub-Or-Rashid, M. S. Satu, S. R. Tammim, F. A. Sunny, and M. A. Moni, "Machine learning and deep learning algorithms in detecting COVID-19 utilizing medical images: a comprehensive review," *Iran Journal of Computer Science*, pp. 1-23, 2024, doi: 10.1007/s42044-024-00190-z.




- [15] R. Prince, Z. Niu, Z. Y. Khan, M. Emmanuel, and N. Patrick, "COVID-19 detection from chest X-ray images using CLAHE-YCrCb, LBP, and machine learning algorithms," *BMC bioinformatics*, vol. 25, no. 1, pp. 28, 2024, doi: 10.1186/s12859-023-05427-5.
- [16] G. Ramasamy, T. Singh, and X. Yuan, "Multi-modal semantic segmentation model using encoder based Link-Net architecture for BraTS 2020 challenge," *Procedia Computer Science*, vol. 218, pp. 732-740, 2023, doi: 10.1016/j.procs.2023.01.053.
- [17] O. M. Al Okashi, I. T. Ahmed, and L. H. Abed, "COVID-19 detection based on combined domain features," *Indonesian Journal of Electrical Engineering and Computer Science*, vol. 26, no. 2, pp. 965-973, 2022, doi: 10.11591/ijeecs.v26.i2.pp965-973.
- [18] I. Ahmed, A. Ahmad, and G. Jeon, "An IoT-based deep learning framework for early assessment of COVID-19," *IEEE Internet of Things Journal*, vol. 8, no. 21, pp. 15855-15862, 2020, doi: 10.1109/jiot.2020.3034074.
- [19] F. Ucar, and D. Korkmaz, "COVIDDiagnosis-net: Deep Bayes-squeezenet based diagnostic of the coronavirus disease 2019 (COVID-19) from X-ray images," *Medical Hypotheses*, vol. 140, Jul. 2020, doi: 10.1016/j.mehy.2020.109761.
- [20] R. Karthik, R. Menaka, and M. J. A. S. C. Hariharan, "Learning distinctive filters for COVID-19 detection from chest X-ray using shuffled residual CNN," *Applied Soft Computing*, vol. 99, pp. 106744, 2021, doi: 10.1016/j.asoc.2020.106744.
- [21] Z. Yang, L. Zhao, S. Wu, and C. Y. Chen, "Lung Lesion Localization of COVID-19 From Chest CT Image: A Novel Weakly Supervised Learning Method," *IEEE Journal of Biomedical and Health Informatics*, vol. 25, no. 6, pp. 864-1872, 2021, doi: 10.1109/jbhi.2021.3067465.
- [22] K. Akyol and B. Şen, "Automatic detection of covid-19 with bidirectional LSTM network using deep features extracted from chest x-ray images," *Interdisciplinary Sciences: Computational Life Sciences*, vol. 14, no. 1, pp. 89-100, 2022, doi: 10.1007/s12539-021-00463-2.
- [23] B. Gülmez, "A novel deep neural network model based Xception and genetic algorithm for detection of COVID-19 from X-ray images," *Annals of Operations Research*, vol. 328, no. 1, pp. 617-641, 2023, doi: 10.1007/s10479-022-05151-y.
- [24] H. Abubakar, F. Al-Turjman, Z. S. Ameen, A. S. Mubarak, and C. Altrjman, "A hybridized feature extraction for COVID-19 multi-class classification on computed tomography images," *Heliyon*, vol. 10, no. 5, 2024, doi: 10.1016/j.heliyon.2024.e26939.
- [25] H. Zhang *et al.*, "Cerebrovascular segmentation in MRA via reverse edge attention network," In *Medical Image Computing and Computer Assisted Intervention-MICCAI 2020: 23rd International Conference, Lima, Peru, October 4-8, 2020, Proceedings, Part VI* 23, pp. 66-75, 2020, doi: 10.1007/978-3-030-59725-2_7.

BIOGRAPHIES OF AUTHORS



Fareesa Amina    received her B.Tech., M.Tech. from Nimra College of Engineering and Technology Ibrahim Patnam Vijaywada Andhra Pradesh Pursuing part time Ph.D–Electronics and Communication Engineering (Ph.D–PT EXT) Register no-ECE06PHD2021 from Bharatiya Engineering Science and Technology innovation University (BESTIU) Gownivasipally, Gorantla Mandal Sri Satya Sai District, Andhra Pradesh India and Working as an Assistant Professor in Shadan Women's College of engineering and technology since 10 years. She can be contacted at email: fareesaameena@gmail.com.



Dr. Krishnanaik Vankdoth B.E. (ECE), M.Tech. (ECE), Ph.D. (ECE).    working as a Professor at Jntuh Affiliated Colleges in India and Ethiopia with 22 years of Teaching, Research and Industrial Experience Supervisor at Bharatiya Engineering Science and Technology Innovation University (Bestiu), Gownivaripalli, Gorantla Mandal, Sri Satya Sai District, Andhra Pradesh. He published 7 International Books, 4 Awards, 30 Memberships, 30 Papers, attended 30 Seminar and Workshop Including One Patent. He can be contacted at email: krishnanaik.ece@gmail.com.